Signal, Image and Video Processing (2022) 16:1127–1133
https://doi.org/10.1007/s11760-021-02062-6

ORIGINAL PAPER

Hyperspectral image denoising with enhanced multivariance product representation

Evrim Korkmaz Özay[1] · **Burcu Tunga**[2]

Received: 31 August 2021 / Revised: 20 October 2021 / Accepted: 23 October 2021 / Published online: 9 January 2022

Abstract
Hyperspectral images are used in many different fields due to their ability to capture wide areas and rich spectrality. However, applications on hyperspectral image (HSI) are affected or limited by various types of noise. Therefore, denoising is an important pre-processing technique for HSI analysis. Tensor decomposition-based denoising algorithms are frequently used due to constraints of traditional two-dimensional methods. An alternative tensor decomposition, enhanced multivariance product representation (EMPR) has been derived from high-dimensional model representation (HDMR) for multivariate functions and discretized for tensor-type data sets. In this study, EMPR-based denoising method is proposed for HSI denoising. EMPR is a decomposition method which is easy to compute and does not include a rank problem that exists in the other tensor decomposition methods. The performance of EMPR-based denoising is evaluated by means of simulated and real experiments on different HSI data sets which include different types of noise. The obtained results are compared with the state-of-the-art tensor-based methods.

Keywords Hyperspectral image · Denoising · Tensor decomposition · Enhanced multivariance product representation

1 Introduction

Hyperspectral imaging has gained great importance with the development of remote sensing technologies in recent years. A hyperspectral image (HSI) is obtained by measuring energy reflection through hundreds of continuously narrow wavelength bands. These images are used for different applications, such as environmental monitoring, agriculture, and defense systems [1,2]. HSI applications in the mentioned areas generally focus on problems like classification, target-anomaly detection and spectral unmixing [3–5]. The performance of HSI applications is limited due to degradation on HSI by several types of noise caused by sensor malfunction or atmospheric effects. Therefore, denoising is an important pre-processing technique for HSI analysis. Traditional HSI denoising methods apply denoising onto each band one by one owing to the fact that each band is a grayscale image. The 2D methods ignore spatial–spectral correlation and denoising capacity of these 2D methods may be limited [6]. Transformation-based methods like Fourier transform or wavelet transform are also used to exploit spatial–spectral correlation in denoising [7]. On the other hand, recent studies which are based on low-rank matrix decomposition achieve better performance for the reconstruction of noisy HS images [8–10]. Low-rank methods capture spectral information successfully but they may cause spatial distortion in denoising.

Researchers investigated tensor decomposition-based techniques to enhance denoising quality, owing to the fact that an HSI can naturally be represented by a tensor [11]. Spatial–spectral correlation of the HSI can be captured more efficiently by some certain tensor decomposition techniques like CANDECOMP/ PARAFAC (CP) decomposition [12] and Tucker decomposition [13]. One of the proposed denoising studies that uses Tucker decomposition is a low-rank tensor approximation (LRTA) method, which provides spatial low-rank approximation, and spectral dimensionality reduction simultaneously [14]. Tucker decomposition is also used for learning overcomplete dictionaries of HSI data sets

✉ Evrim Korkmaz Özay
evrimozay@beykent.edu.tr

Burcu Tunga
tungab@itu.edu.tr

[1] Software Engineering Department, Faculty of Engineering-Architecture, Beykent University, Sarıyer 34398, İstanbul, Turkey

[2] Mathematics Engineering Department, Faculty of Arts and Sciences, İstanbul Technical University, Maslak 34469, İstanbul, Turkey

and these dictionaries were used in denoising problem as tensor dictionary learning (TDL) [15]. Another denoising method on tensor decomposition is hyper-Laplacian regularized unidirectional low-rank tensor recovery (LLRT) [16] which is not efficient on mixed noise as on Gaussian noise. CP decomposition, also known as PARAFAC, is a commonly used algorithm for HSI denoising, which may lead to spectral distortion due to the estimation of the CP rank that is dependent on variance of noise [17,18]. In addition, other commonly used tensor decomposition techniques have not only similar problems, but also high computational complexity.

This paper proposes a statistical tensor decomposition method for HSI denoising, enhanced multivariance product representation (EMPR), unlike the other tensor-based methods which are the subjects of multivariate linear algebra. EMPR is a divide-and-conquer algorithm which is based on Sobol's high-dimensional model representation (HDMR) [19]. Recently, EMPR has been used to solve different problems in image processing [20,21]. Compared with the other tensor-based denoising methods, our main contributions are as follows:

- EMPR is capable of capturing spatial–spectral correlation with components that have less dimension than the HSI. This feature of EMPR empowers denoising performance on mixed-type noise.
- EMPR's components are easy to compute and certain components which are called "support vectors" can be calculated flexibly with prior knowledge, if there is any, of the noise model.
- EMPR is a statistical representation of a multivariate function which can be used as a dimensionality reduction method. EMPR's components can be easily evaluated with marginal expectations under support and weight functions. Therefore, EMPR-based denoising is computationally more efficient than the other tensor-based denoising methods.

This paper is organized as follows: The next section gives an explanation on the mathematical background of EMPR. Section 3 clarifies how to use the EMPR algorithm to remove noise on HSI. We carried out simulated and real experiments in Sect. 4 to show compared quantitative and illustrative assessments. Section 5 concludes the study and informs readers on future works.

2 Enhanced multivariance product representation

EMPR is a dimensionality reduction method for expressing an N-direction tensor in terms of less-dimensional tensors and certain support vectors. Using EMPR method, the element with index $i_1 \dots i_N$ of the N-dimensional tensor structure $\mathcal{X}$ can be expressed as follows.

$$\begin{aligned}\mathcal{X}_{i_1\dots i_N} &= \mathcal{X}^{(0)} \prod_{j=1}^{N} s_{i_j}^{(j)} + \sum_{j_1=1}^{N} \mathcal{X}_{i_{j_1}}^{(j_1)} \prod_{\substack{j=1\\ j\neq j_1}}^{N} s_{i_j}^{(j)} \\ &+ \sum_{\substack{j_1,j_2=1\\ j_1<j_2}}^{N} \mathcal{X}_{i_{j_1},i_{j_2}}^{(j_1 j_2)} \prod_{\substack{j=1\\ j\neq j_1,j_2}}^{N} s_{i_j}^{(j)} + \cdots + \mathcal{X}_{i_{j_1} i_{j_2}\dots i_{j_N}}^{(j_1 j_2 \dots j_N)}, \\ & i_j = 1, 2, \dots, n_j, \quad j = 1, 2, \dots, N. \end{aligned} \tag{1}$$

Here, $\mathcal{X}^{(0)}$ is a constant, $\mathcal{X}^{(j_1)}$s are one-way tensors (or vectors), and $\mathcal{X}^{(j_1 j_2)}$s are two-way tensors, that is, matrices. The right hand side components can be considered as tensors of increasing number of dimensions. So the last element $\mathcal{X}^{(j_1 j_2 \dots j_N)}$ is the N-way tensor. This expansion contains a finite number of sums. $s^{(j)}$s in the expansion are called support vectors. The main purpose of this method is to determine the general structures of EMPR's components using support vectors and to represent the multivariate data with less variate components. To calculate the components in EMPR expansion, a weight vector $(W_{i_j}^{(j)})$ is used in each direction. This weight vector satisfies the normalization conditions given below.

$$\begin{aligned}\sum_{i_j=1}^{n_j} W_{i_j}^{(j)} = 1, \quad \sum_{i_j=1}^{n_j} W_{i_j}^{(j)} \left(s_{i_j}^{(j)}\right)^2 = 1, \\ j = 1, 2, \dots, N. \end{aligned} \tag{2}$$

To uniquely obtain the EMPR components, vanishing conditions are defined over the weight and support vectors as follows

$$\begin{aligned}\sum_{i_{j_l}=1}^{n_{j_l}} W_{i_{j_l}}^{(j_l)} s_{i_{j_l}}^{(j_l)} \mathcal{X}_{i_{j_1}\dots i_{j_k}}^{(j_1\dots j_k)} = 0, \\ l = 1, 2, \dots, k, \quad k = 1, 2, \dots, N. \end{aligned} \tag{3}$$

Under the conditions described above, the constant component of the EMPR expansion, $\mathcal{X}^{(0)}$ can be calculated as follows.

$$\mathcal{X}^{(0)} = \sum_{i_1=1}^{n_1} \cdots \sum_{i_N=1}^{n_N} \left[\prod_{k=1}^{N} W_{i_k}^{(k)} s_{i_k}^{(k)}\right] \mathcal{X}_{i_1\dots i_N}. \tag{4}$$

The univariate components denoted by $\mathcal{X}^{(j)}$ are calculated with the exclusion of the relevant direction.

$$\begin{aligned}\mathcal{X}_{i_j}^{(j)} = \sum_{i_1=1}^{n_1} \cdots \sum_{i_{j-1}=1}^{n_{j-1}} \sum_{i_{j+1}=1}^{n_{j+1}} \cdots \sum_{i_N=1}^{n_N} \left[\prod_{\substack{k=1\\ j\neq k}}^{N} W_{i_k}^{(k)} s_{i_k}^{(k)}\right] \\ \times \mathcal{X}_{i_1\dots i_N} - \mathcal{X}^{(0)} s_{i_j}^{(j)} \\ i_j = 1, 2, \dots, n_j, \quad j = 1, 2, \dots, N. \end{aligned} \tag{5}$$

Bivariate components are similarly calculated excluding the two related directions as follows.

$$\mathcal{X}_{i_j,i_k}^{(j,k)} = \sum_{i_1=1}^{n_1} \cdots \sum_{i_{j-1}=1}^{n_{j-1}} \sum_{i_{j+1}=1}^{n_{j+1}} \cdots \sum_{i_{k-1}=1}^{n_{k-1}} \sum_{i_{k+1}=1}^{n_{k+1}} \cdots$$

$$\cdots \sum_{i_N=1}^{n_N} \left[\prod_{\substack{k=1 \\ j\neq k}}^{N} W_{i_k}^{(k)} s_{i_k}^{(k)} \right] \mathcal{X}_{i_1 \ldots i_N} - \mathcal{X}_{i_k}^{(k)} s_{i_j}^{(j)} - \mathcal{X}_{i_j}^{(j)} s_{i_k}^{(k)} - \mathcal{X}^{(0)} s_{i_j}^{(j)} s_{i_k}^{(k)}, \quad j,k = 1,2,\ldots,N, \quad i_j = 1,2,\ldots,n_j, \quad i_k = 1,2,\ldots,n_k. \tag{6}$$

The other EMPR components at the right hand side of Eq. 1 are calculated in a similar way.

It is important to determine the support vectors in the EMPR method since it directly affects the performance of the method. Although there is no restriction on the evaluation of the support vectors, it is well known from the previous studies that the calculation of the support vectors by normalizing the directional averages of the data set has produced good results [23]. For this reason, the support vectors obtained in this way are used in this study, and their mathematical definition is given below.

$$s_{i_j}^{(j)} = \frac{\sum_{i_1=1}^{n_1} \cdots \sum_{i_{j-1}=1}^{n_{j-1}} \sum_{i_{j+1}=1}^{n_{j+1}} \cdots \sum_{i_N=1}^{n_N} \mathcal{X}_{i_1 \ldots i_N}}{\left[\sum_{i_j=1}^{n_j} \left[\sum_{i_1=1}^{n_1} \cdots \sum_{i_{j-1}=1}^{n_{j-1}} \sum_{i_{j+1}=1}^{n_{j+1}} \cdots \sum_{i_N=1}^{n_N} \mathcal{X}_{i_1 \ldots i_N} \right]^2 \right]^{\frac{1}{2}}}. \tag{7}$$

In the next section, it is explained how noise can be removed in HSI by using EMPR components.

3 Proposed method

The mathematical expression of a noisy HSI is as follows

$$\mathcal{Y} = \mathcal{X} + \mathcal{N} \tag{8}$$

where $\mathcal{Y}$, $\mathcal{X}$ and $\mathcal{N}$ are the observed noisy HSI, noise-free HSI and noise tensor, respectively. All are three-way tensors with the same dimension, (n_1, n_2, n_3). Due to the multi-band nature of HSI, 2D denoising methods may cause image distortions or artifacts. The main reason for this is that such traditional methods are effective only in spatial dimensions and are inefficient at capturing correlated structures through the bands. In the EMPR method, the spatial relationship between the pixels as well as the relationship between the bands is included in the HSI data representation through the EMPR components. In other words, if the spatial coordinates of the first and second directions are indexed by i, j and the spectral coordinate of the third direction (band order) is indexed by k in the HSI containing noise, the three-way component of the EMPR method, $\mathcal{Y}^{(1,2,3)}$, and the two-way components, $\mathcal{Y}^{(1,2)}$, $\mathcal{Y}^{(1,3)}$ and $\mathcal{Y}^{(2,3)}$, define a statistical relationship between spatial and spectral dimensions in different directions. These EMPR components can be considered as high-frequency components in multi-resolution analysis-based methods and some of these high-frequency components are loaded by heavy noise.

The element in the $\{i, j, k\} - th$ position of this HSI data set can be expressed exactly by the EMPR method with the following equation.

$$\begin{aligned} \mathcal{Y}_{i,j,k} &= \mathcal{Y}^{(0)} s_i^{(1)} s_j^{(2)} s_k^{(3)} + \mathcal{Y}_i^{(1)} s_j^{(2)} s_k^{(3)} \\ &+ \mathcal{Y}_j^{(2)} s_i^{(1)} s_k^{(3)} + \mathcal{Y}_k^{(3)} s_i^{(1)} s_j^{(2)} + \mathcal{Y}_{i,j}^{(1,2)} s_k^{(3)} \\ &+ \mathcal{Y}_{i,k}^{(1,3)} s_j^{(2)} + \mathcal{Y}_{j,k}^{(2,3)} s_i^{(1)} + \mathcal{Y}_{i,j,k}^{(1,2,3)} \\ i &= 1,2,\ldots,n_1, \quad j = 1,2,\ldots,n_2, \quad k = 1,2,\ldots,n_3. \end{aligned} \tag{9}$$

To develop a novel denoising method using the EMPR method, some high-frequency terms have been extracted from the EMPR expansion of the HSI. For this purpose, the components, $\mathcal{Y}_{i,j,k}^{(1,2,3)}$, $\mathcal{Y}_{i,k}^{(1,3)}$ and $\mathcal{Y}_{j,k}^{(2,3)}$, are excluded from the element in the $\{i, j, k\} - th$ position of this HSI which is $\mathcal{Y}_{i,j,k}$ as follows

$$\begin{aligned} \mathcal{X}_{i,j,k} &\approx \mathcal{Y}_{i,j,k} - \mathcal{Y}_{i,j,k}^{(1,2,3)} - \mathcal{Y}_{i,k}^{(1,3)} - \mathcal{Y}_{j,k}^{(2,3)} \\ i &= 1,2,\ldots,n_1, \quad j = 1,2,\ldots,n_2, \quad k = 1,2,\ldots,n_3 \end{aligned} \tag{10}$$

From another point of view, the high-frequency EMPR terms $\mathcal{Y}_{i,j,k}^{(1,2,3)}$, $\mathcal{Y}_{i,k}^{(1,3)}$ and $\mathcal{Y}_{j,k}^{(2,3)}$ are taken as noise and the results suggest that EMPR was relatively successful in the tests. The performance of the proposed method and the results of the comparison between the other state-of-the-art tensor-based denoising methods are given in the next section.

4 Experimental design and analysis

4.1 Experimental design

EMPR's denoising performance is compared with PARAFAC, LRTA, TDL, and LLRT which all are tensor-based denoising methods. For quantitative assessment, peak signal-to-noise ratio (PSNR), relative dimensionless global error in synthesis (ERGAS), the structural similarity (SSIM), and spectral angle mapper (SAM) are chosen as evaluation metrics [24]. Larger values of PSNR and SSIM indicate better denoising performance. Smaller values of ERGAS and SAM point out high performance in denoising. Two types of experiments are designed for the assessment of the proposed method. The first type of experiment is simulated on two different HSI data sets. The second type of experiment is the

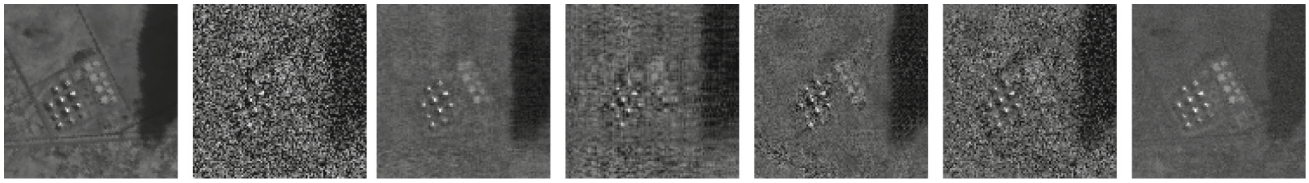

(a) Original band **(b)** Noisy band **(c)** PARAFAC **(d)** LRTA **(e)** TDL **(f)** LLRT **(g)** EMPR

Fig. 1 Denoising results for band 50 of Abu-Urban data set

Table 1 Quantitative Assessment of Denoising Performance for Abu-Urban

Method	ERGAS	MPSNR	MSSIM	SAM
Noisy HSI	87.4082	16.0103	0.0963	0.8863
PARAFAC	25.5157	**29.3575**	0.6033	0.4049
LRTA	31.5548	24.8371	0.3615	0.4751
TDL	37.0973	26.2579	0.4393	0.4565
LLRT	62.2970	19.7582	0.1781	0.7027
EMPR	**16.3073**	27.4384	**0.6490**	**0.3963**
Ideal Value	0	∞	1	0

Table 2 Running Time for Abu-Urban

Method	PARAFAC	LRTA	TDL	LLRT	EMPR
Time(sec)	169.2491	2.8776	7.6621	288.7012	**1.3319**

visual comparison of denoising performance of EMPR on a real HSI. For the simulated experiment, the ABU-Urban and the ABU-Airport[1] from AVIRIS (Airborne Visible/Infrared Imaging Spectrometer) are chosen [25]. The Abu-Airport data set consists of 100 × 100 pixels with 205 bands while Abu-Urban has the same dimensions and 207 bands. For the real data experiment, Urban[2] data set has been chosen.

4.2 Simulated experiments

Abu-Urban data set is chosen for the first simulated experiment. The noise model for this experiment includes zero-mean Gaussian noise with different standard deviation randomly sampled from [0.1,0.2] for each band, and randomly selected 20 bands were added noise with 20% density salt and pepper noise. Table 1 shows ERGAS, mean PSNR, mean SSIM, and SAM, respectively, for different tensor-based denoising methods. The results are given for the mean of twenty runs. The best results in Tables 1–4 for each quality metric are marked in bold and the second best results are underlined. According to the results given in this table, it is clear that EMPR outperforms for three quality indexes and it is the second best for MPSNR. Table 2 gives the running time and EMPR is the fastest denoising method among them all.

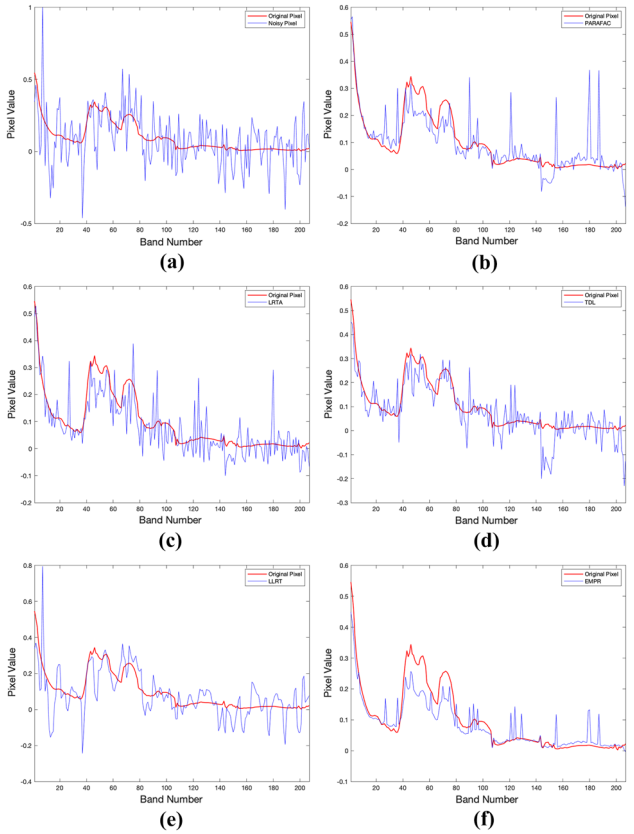

Fig. 2 Spectral signature restoration of different methods for the pixel in [15,45] of Abu-Urban. **a** Noisy pixel, **b** PARAFAC, **c** LRTA, **d** TDL, **e** LLRT, **f** (EMPR)

Figure 1 presents visual quality of denoising performance for each tensor-based method on Abu-Urban data set. The results are given for band 50 of the simulated HSI. The outputs of LRTA and LLRT algorithms are still noisy. PARAFAC and TDL yield better visional results, however, EMPR is demonstrably superior denoiser.

Spectra of a selected noisy pixel from Abu-Urban data set along with reconstruction results are illustrated in Fig. 2. EMPR provides better suppression of noise while repre-

[1] http://xudongkang.weebly.com/data-sets.html

[2] https://rslab.ut.ac.ir/data

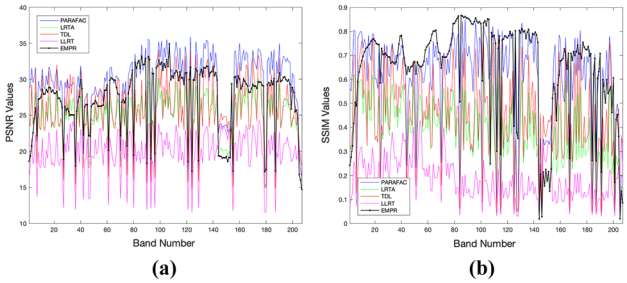

(a) (b)

Fig. 3 PSNR and SSIM values of different denoising methods in each band of the first simulated experiment on Abu-Urban

Table 3 Quantitative Assessment of Denoising Performance for Abu-Airport

Method	ERGAS	MPSNR	MSSIM	SAM
Noisy HS	67.4316	14.8619	0.1159	0.7983
PARAFAC	37.3634	27.2129	0.6776	0.4679
LRTA	43.2151	21.1609	0.3302	0.5387
TDL	41.6326	23.1975	0.52088	0.5208
LLRT	40.6130	18.2982	0.0229	0.6747
EMPR	**19.1255**	**29.2417**	**0.8134**	**0.2578**
Ideal Value	0	∞	1	0

Table 4 Running Time for Abu-Airport

Method	PARAFAC	LRTA	TDL	LLRT	EMPR
Time(sec)	162.4416	3.5995	6.0819	300.0680	**1.2553**

senting pixel spectra. However, there are slight numerical differences between band 40 and band 100 for EMPR's reconstruction as seen in Fig. 2f. Figure 3 presents PSNR and SSIM values through the bands, respectively. PSNR values are lower than PARAFAC, which is compatible with MPSNR results in Table 1.

The simulated experiment on the Abu-Airport data set is designed with four different types of noise to show the performance of the proposed method [22]. This consists of zero-mean Gaussian noise with different standard deviations randomly sampled from $[0.1, 0.2]$ for each band, impulse noise with 20% density percentage for randomly 20 selected bands, dead lines with a width from 1 to 3 were added to 20% of the bands, which were randomly selected and stripes with a width from 6 to 15 were added to a randomly selected 40% of the bands. Table 3 indicates that EMPR effectively removes the mixed noise compared to the other methods. Figure 4 presents visual results which are compatible with quantitative results in the table. Figure 4 points out that all the methods except EMPR do not accomplish the removal of stripes. Running time of the methods are presented in Table 4.

Restoration of a noisy pixel for all of the methods is given in Fig. 5. EMPR-based denoising fluctuates less than the other methods and achieves better approximation to the original pixel.

PSNR and SSIM values are given in Fig. 6. As it can be seen in the figure, EMPR provides lower PSNR values than PARAFAC in the vast majority of the first fifty bands.

4.3 Experiment on real data

Urban data set is used to verify denoising performance of EMPR on HSI. This data set has some degradation due to noisy bands. A subscene of this data set with 150×150 size is cropped where the noise is dense and includes stripes. This data set has 210 bands. Bands 139 and 208 are corrupted by heavy noise. Figures 7 and 8 show visual results of denoising on bands 139 and 208, respectively. According to the visual results of the restored bands, EMPR has superiority over the other tensor-based methods.

4.4 Discussion

According to the experiments with both simulated and real data, it can be concluded that EMPR is particularly effective at HSI denoising. Bivariate and trivariate EMPR components have spatial–spectral correlation for different directions of HSI data cube. We excluded EMPR's most noisy compo-

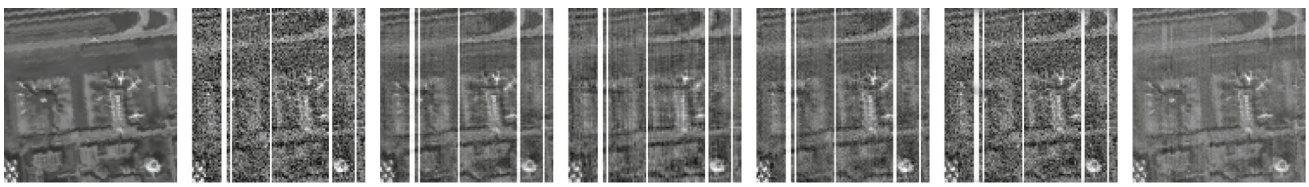

(a) Original band 20 **(b)** Noisy band 20 **(c)** CP **(d)** LRTA **(e)** TDL **(f)** LLRT **(g)** EMPR

Fig. 4 Denoising results for band 20 of Abu-Airport data set

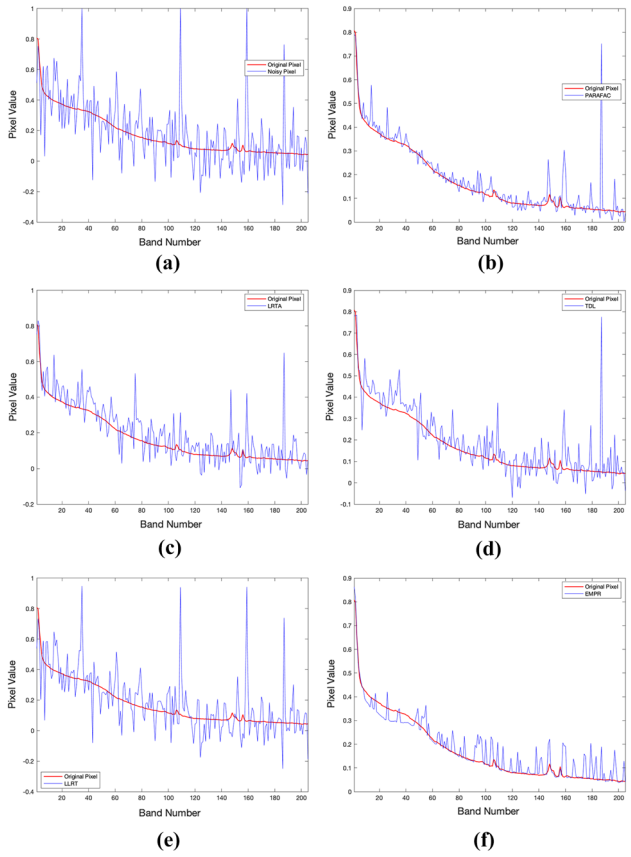

Fig. 5 Spectral signature restoration of different methods for the pixel in [45,89] of Abu-Airport-3. **a** Noisy pixel, **b** PARAFAC, **c** RTA, **d** TDL, **e** LLRT, **f** (EMPR)

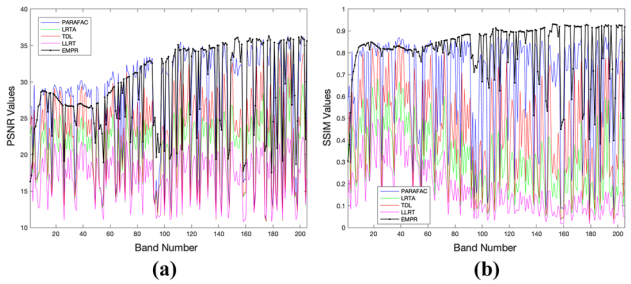

Fig. 6 PSNR and SSIM values of different denoising methods in each band of the simulated experiment-1 on Abu-Airport

nents for the denoising process. As pointed out in Sect. 4.2, there are some numerical differences for some of the bands at EMPR-based denoising. These results potentially demonstrate that EMPR's components may not be able to capture the spectrality totally on these bands of the HSI signals. Another topic of discussion is EMPR's PSNR results in Fig. 3. Looking at these results, it can be inferred that EMPR is more sensitive to the Gaussian noise than to the other types of noise, since Gaussian noise added to all of the bands. Nevertheless, it should be noted that EMPR is still the best denoiser considering the other quantitative metrics like SSIM. Moreover, it is clear from the experiments that EMPR provides a better performance on the removal of the mixed-type noise.

5 Conclusion and future work

This article proposes a new HSI denoising method using EMPR. EMPR naturally represents tensor-type data sets by describing different statistical features of different dimensions. The EMPR method makes it easy to process multidimensional data sets through pre-calculated support vectors. These support vectors can be considered as priors of the denoising model. The features of the support vectors and divide-and-conquer mechanism of EMPR allow us to develop an efficient tensor decomposition-based denoising method for HSI. Both simulated and real experiments demonstrated promising results on the EMPR's denoising quality. Running time results also revealed that EMPR has lower computational complexity than the other state-of-the-art tensor-based denoising methods. On the other hand, as discussed in Sect. 4.4, EMPR's sensitivity to the Gaussian noise should be explored in future work. A non-local approach can be utilized to improve EMPR's performance on Gaussian noise and can empower spectrality of the EMPR components. Another future study for consideration is the detailed analysis of EMPR noisy components' spectrality.

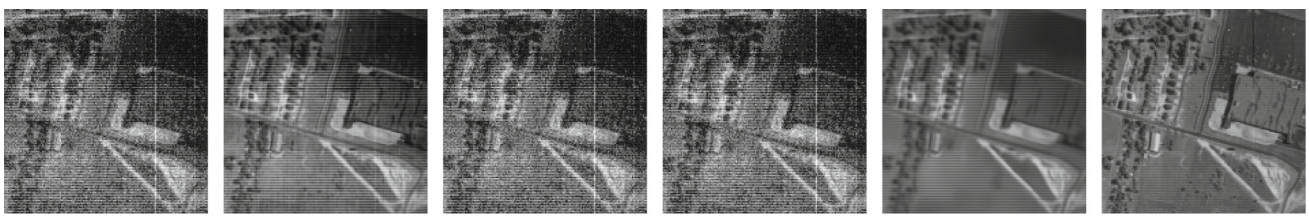

Fig. 7 Urban data set: **a** original band 139, **b** PARAFAC, **c** LRTA, **d** TDL, **e** LLRT, **f** EMPR

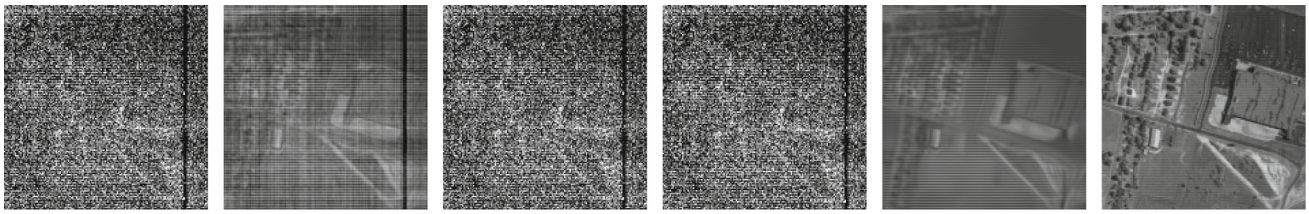

Fig. 8 Urban data set: **a** original band 208, **b** PARAFAC, **c** LRTA, **d** TDL, **e** LLRT, **f** EMPR

References

1. Bioucas-Dias, J.M., Plaza, A., Camps-Valls, G., Scheunders, P., Nasrabadi, N., Chanussot, J.: Hyperspectral remote sensing data analysis and future challenges. IEEE Geosci. Remote Sens. Mag. **1**(2), 6–36 (2013)
2. Khan, M.J., Khan, H.S., Yousaf, A., Khurshid, K., Abbas, A.: Modern trends in hyperspectral image analysis: a review. IEEE Access **6**, 14118–14129 (2018)
3. Ghamisi, P., Plaza, J., Chen, Y., Li, J., Plaza, A.J.: Advanced spectral classifiers for hyperspectral images: a review. IEEE Geosci. Remote Sens. Mag. **5**(1), 8–32 (2017)
4. Nasrabadi, N.M.: Hyperspectral target detection: an overview of current and future challenges. IEEE Signal Process. Mag. **31**(1), 34–44 (2013)
5. Qian, Y., Xiong, F., Zeng, S., Zhou, J., Tang, Y.Y.: Matrix-vector nonnegative tensor factorization for blind unmixing of hyperspectral imagery. IEEE Trans. Geosci. Remote Sens. **55**(3), 1776–1792 (2016)
6. Dabov, K., Foi, A., Katkovnik, V., Egiazarian, K.: Image denoising by sparse 3-D transform-domain collaborative filtering. IEEE Trans. Image Process. **16**(8), 2080–2095 (2007)
7. Atkinson, I., Kamalabadi, F., Jones, D.L.: Wavelet-based hyperspectral image estimation. In: IEEE International Geoscience and Remote Sensing Symposium, vol. 2, pp. 743–745 (2003)
8. Rasti, B., Scheunders, P., Ghamisi, P., Licciardi, G., Chanussot, J.: Noise reduction in hyperspectral imagery: overview and application. Remote Sens. **10**(3), 482 (2018)
9. Zhuang, L., Bioucas-Dias, J.M.: Fast hyperspectral image denoising and inpainting based on low-rank and sparse representations. IEEE J. Sel. Top. Appl. Earth Obs. Remote Sens. **11**(3), 730–742 (2018)
10. He, W., Zhang, H., Zhang, L., Shen, H.: Hyperspectral image denoising via noise-adjusted iterative low-rank matrix approximation. IEEE J. Sel. Top. Appl. Earth Obser. Remote Sens. **8**(6), 3050–3061 (2015)
11. Lin, T., Bourennane, S.: Survey of hyperspectral image denoising methods based on tensor decompositions. EURASIP J. Adv. Signal Process. **2013**, 1–11 (2013)
12. Veganzones, M.A., Cohen, J.E., Farias, R.C., Chanussot, J., Comon, P.: Nonnegative tensor CP decomposition of hyperspectral data. IEEE Trans. Geosci. Remote Sens. **54**(5), 2577–2588 (2015)
13. Chen, Y., He, W., Yokoya, N., Huang, T.Z.: Hyperspectral image restoration using weighted group sparsity-regularized low-rank tensor decomposition. IEEE Trans. Cybern. **50**(8), 3556–3570 (2019)
14. Renard, N., Bourennane, S., Blanc-Talon, J.: Denoising and dimensionality reduction using multilinear tools for hyperspectral images. IEEE Geosci. Remote Sens. Lett. **5**(2), 138–142 (2008)
15. Zubair, S., Wang, W.: Tensor dictionary learning with sparse tucker decomposition. In: 18th International Conference on Digital Signal Processing (DSP), pp. 1–6, (2013)
16. Chang, Y., Yan, L., Zhong, S.: Hyper-laplacian regularized unidirectional low-rank tensor recovery for multispectral image denoising. In: Proc. IEEE Conf. Comput. Vis. Pattern Recognit. (CVPR), pp. 4260–4268 (2017)
17. Liu, X., Bourennane, S., Fossati, C.: Denoising of hyperspectral images using the PARAFAC model and statistical performance analysis. IEEE Trans. Geosci. Remote Sens. **50**(10), 3717–3724 (2012)
18. Xue, J., Zhao, Y., Liao, W., Chan, J.C.W.: Nonlocal low-rank regularized tensor decomposition for hyperspectral image denoising. IEEE Trans. Geosci. Remote Sens. **57**(7), 5174–5189 (2019)
19. Sobol, I.M.: Theorems and examples on high dimensional model representation. Reliab. Eng. Syst. Saf. **79**(2), 187–193 (2003)
20. Özay, E.K., Demiralp, M.: Combined small scale enhanced multivariance product representation (CSSEMPR) for image reconstruction. In: AIP Conference Proceedings, vol. 1702(1) (2015)
21. Tuna, S., Töreyin, B.U., Demiralp, M., Ren, J., Zhao, H., Marshall, S.: Iterative enhanced multivariance products representation for effective compression of hyperspectral images. IEEE Trans. Geosci. Remote Sens. **59**(11), 9569–9584 (2021)
22. Wang, M., Wang, Q., Chanussot, J., Li, D.: Hyperspectral image mixed noise removal based on multidirectional low-rank modeling and spatial-spectral total variation. IEEE Trans. Geosci. Remote Sens. **59**(1), 488–507 (2020)
23. Tunga, M.A.: A new approach for multivariate data modelling in orthogonal geometry. Int. J. Comput. Math. **92**(9), 2011–2021 (2015)
24. Jagalingam, P., Hegde, A.V.: A review of quality metrics for fused image. Aquatic Procedia **4**, 133–142 (2015)
25. Kang, X., Zhang, X., Li, S., Li, K., Li, J., Benediktsson, J.A.: Hyperspectral anomaly detection with attribute and edge-preserving filters. IEEE Trans. Geosci. Remote Sens. **55**(10), 5600–5611 (2017)